JOURNAL OF GEOPHYSICAL RESEARCH: SPACE PHYSICS, VOL. 118, 1837–1848, doi:10.1002/jgra.50235, 2013

An observation-based GCR model of heavy nuclei: Measurements from CRIS onboard ACE spacecraft

L.-L. Zhao[1] and G. Qin[1]

Received 13 October 2012; revised 6 March 2013; accepted 10 March 2013; published 10 May 2013.

[1] We present an observation-based elemental Galactic Cosmic Ray (GCR) heavy nuclei spectra model, based on ACE/CRIS measurements. Then we extrapolate the spectra model to the lower energy range of ACE/SIS instrument. In addition, we compare the modeling results with both the CRIS and SIS measurements. The flux of lower energetic particles measured by SIS are despiked since there are Solar Energetic Particle (SEP) events. The good agreement between the modeling and the observation results, especially for the solar minimum, indicates the validity of our model in the energy range 30–500 MeV/nuc. Compared with two GCR radiation environment models, CRÈME96/Nymmik model and Badhwar & O'Neill model, our model can provide an improved fit to the GCRs spectra measured by ACE. Furthermore, our model is a phenomenological one, without consideration of the physical process during GCRs' propagating through the heliosphere. Therefore, it is more straightforward and applicable in practice. Finally, the model can reproduce and predict the GCR spectra in the past and future, respectively, based on the strong correlation between the model parameters and solar activity indicated by sunspot number.

Citation: Zhao, L.-L., and G. Qin (2013), An observation-based GCR model of heavy nuclei: Measurements from CRIS onboard ACE spacecraft, *J. Geophys. Res. Space Physics*, *118*, 1837–1848, doi:10.1002/jgra.50235.

1. Introduction

[2] The heavy nuclei of Galactic Cosmic Ray (GCR) provide very important information about cosmic ray's origin, acceleration mechanism, as well as propagation and modulation processes in the heliosphere through their elemental and isotopic composition. It is well established that GCR flux correlates inversely with solar activity [*McDonald*, 1998]. The numerical modeling of GCR modulation in the heliosphere has also made significant progress over the past several decades [*Fichtner*, 2005]. For instance, the advanced 2-D or 3-D models based on solving Parker's transport equation (e.g., finite-difference method [*Jokipii and Kopriva*, 1979; *Kota and Jokipii*, 1983] and stochastic method [*Zhang*, 1999; *Qin et al.*, 2006; *Pei et al.*, 2010]) are remarkably successful in reconciling observation from various spacecraft, balloon experiments and ground-based stations. However, a comprehensive understanding of the GCR heavy nuclei remains challenging, partly attributed to the fact that the intensities of heavy nuclei in GCR are relatively low and highly variable in space and time, hence, the progress in the past has been impeded by limited particle collection ability.

[3] In addition, accurate knowledge of GCR abundances and energy spectra of heavy ions may protect astronauts in the long-duration deep space missions, as well as sensitive electronic instruments, from the radiation hazard. In spite of their relatively low abundance, the heavy nuclei contribute significantly to the total radiation dose, especially with energy below 1 GeV/nuc due to the fact that they have a high rate of ionization energy loss [*Davis et al.*, 2001]. *Wilson et al.* [1997] estimated that the heavy nuclei account for approximately half of the blood-forming organs dose equivalent behind 5 g/cm^2 of aluminum shielding at solar minimum, with significant contribution from relatively abundant heavy ions, e.g., C, N, O, Ne-S, Fe. Since the low-energy heavy ions are easy to shield against, the heavy ions with energy above 30 MeV/nuc are the major contributor to cancer and other health risks from space radiation due to their large ionization power [*Durante and Cucinotta*, 2008, 2011]. Furthermore, although the heavy ions are less penetrating than protons and heliums, they are usually the dominant cause of single event effects (SEEs) in the GCR environment [*Dodd et al.*, 2007].

[4] Fortunately, the NASA Advanced Composition Explorer (ACE) spacecraft has greatly extended our ability to explore the heavy nuclei over a wide energy range, including energy spectra, elemental and isotopic abundances, and the ionic charge of nuclei from H to Ni [*Stone et al.*, 1998a]. The Cosmic Ray Isotope Spectrometer [CRIS, *Stone et al.*, 1998b] onboard ACE has continuously recorded "quiet time" energy spectra for elements with nuclear charge from 5 to 28 over the energy range 50–500 MeV/n since its launch in August, 1997. The measurement from CRIS are highly statistically significant due

[1]College of Earth Sciences, University of Chinese Academy of Sciences, Beijing, China.

Corresponding author: L.-L. Zhao, State Key Laboratory of Space Weather, Center for Space Science and Applied Research, Chinese Academy of Sciences, P.O. Box 8701, Beijing 100190, China. (llzhao@spaceweather.ac.cn)

2169-9380/13/10.1002/jgra.50235

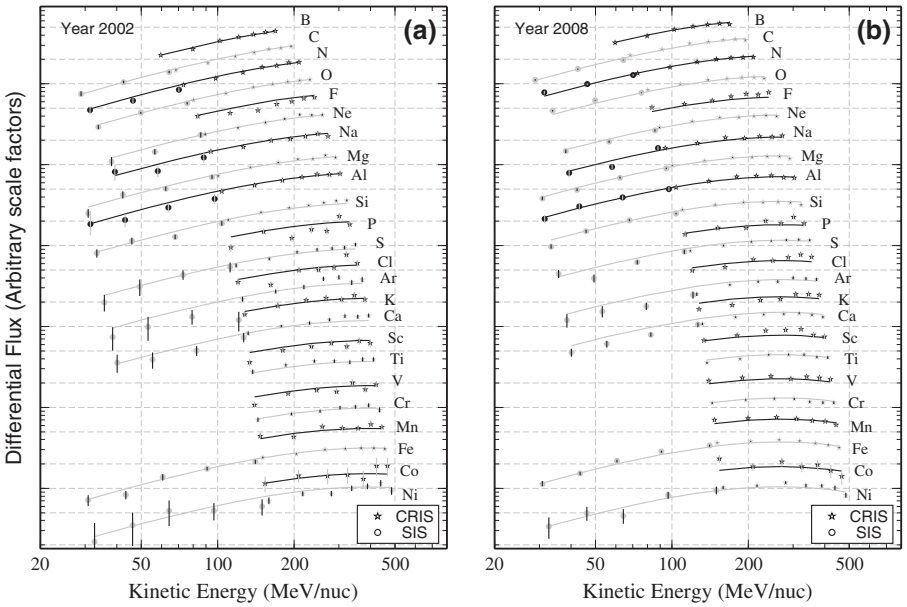

Figure 1. Observed elemental GCR spectra from boron to nickel from ACE/SIS (circles) and ACE/CRIS (stars) measurements for (a) solar maximum (year 2002) and (b) solar minimum (year 2008) in the energy range 30 $\sim$ 500 MeV/nuc. The solid curves show the energy spectra from our model. Arbitrary scale factors have been applied to the flux of each element for the presentation of the spectral shape. Vertical bars denote the statistically standard error.

to its large geometrical acceptance and excellent charge and mass resolution. The data sets with unprecedented statistical precision from CRIS and other instruments onboard ACE have greatly improved our knowledge about heavy ions [*Davis et al.*, 2001; *Wiedenbeck et al.*, 2005; *O'Neill*, 2006; *Mason et al.*, 2008; *George et al.*, 2009; *Mewaldt et al.*, 2010]. *George et al.* [2009] analyzed the measurements of elemental abundances and spectra of heavy nuclei from the boron to nickel obtained by ACE/CRIS during both solar minimum and solar maximum, and concluded that the CRIS data are generally consistent with previous measurements and provides a high-precision baseline for future studies of GCRs, e.g., their composition, solar modulation over the solar cycle, space radiation hazards, etc. And *George et al.* [2009], also using the ACE/CRIS data, showed that intensities of elements consisting primarily of secondaries (produced by cosmic ray fragmentation in the Galaxy) fall off more rapidly going to low energies than do those of primary elements.

[5] Currently, there are several models of the GCR radiation environment commonly used for evaluating radiation hazard, including the "leaky box" model [*Cowsik et al.*, 1967], the CHIME model [*Chenette et al.*, 1994], the Badhwar & O'Neill model [*Badhwar and O'Neill*, 1994, 1996] and CRÈME96/Nymmik model [*Tylka et al.*, 1997]. Among all of these models, the "leaky box" model is the simplest one but can still reproduce the observations with reasonable accuracy. In addition, the CHIME model is specified for the calculation of SEEs due to interplanetary heavy ions. The Badhwar & O'Neill model characterizes the level of solar modulation with a single time-dependent parameter, the modulation potential $\Phi(t)$, which is related to the energy and rigidity required for interstellar particles to propagate through the heliosphere to the observation radius [*Badhwar and O'Neill*, 1996; *O'Neill*, 2006]. Then the modulation potential $\Phi(t)$ is correlated with ground-based nearly continuous neutron monitor counting rates, resulting prediction of $\Phi(t)$ at later times from the regression line. Note that the Badhwar & O'Neill model is a physics-based model, depending on the solar modulation of cosmic rays in the heliosphere including the diffusion-convection mechanism [*Badhwar and O'Neill*, 1996]. However, the CRÈME96/Nymmik model is a phenomenological one that, based on the semi-empirical model of *Nymmik et al.* [1992], and the variations of cosmic ray intensities, are directly related to the sunspot number (SSN), which is a general measure of the level of solar activity [*Tylka et al.*, 1997]. Moreover, for the NM-based reconstruction method, the neutron monitors are sensitive to the reaction products of 1–20 GeV primary cosmic rays in the Earth's atmosphere so that the lower energy part of the GCR spectrum may be underestimated [*Usoskin et al.*, 2011]. Furthermore, the Badhwar and O'Neill model and CRÈME96/Nymmik model are based on the balloon and spacecraft data of varying precision from about three decades before the work was done. Hence, the accuracy of these models is rather limited, and the solar minimum predictions is estimated to deviate from the ACE measurement by as much as 15–20% [*Davis et al.*, 2001, Figure 4], which suggests that both models need revision in light of the high-quality data from ACE. Actually, *O'Neill* [2006, 2010] has updated the original Badhwar-O'Neill Model with the new ACE data to produce more accurate GCR environment data. Furthermore, *George et al.* [2009] showed that a steady state "leaky box" galactic propagation model could give good (but not perfect) fit to the observed spectra from ACE/CRIS with different modulation

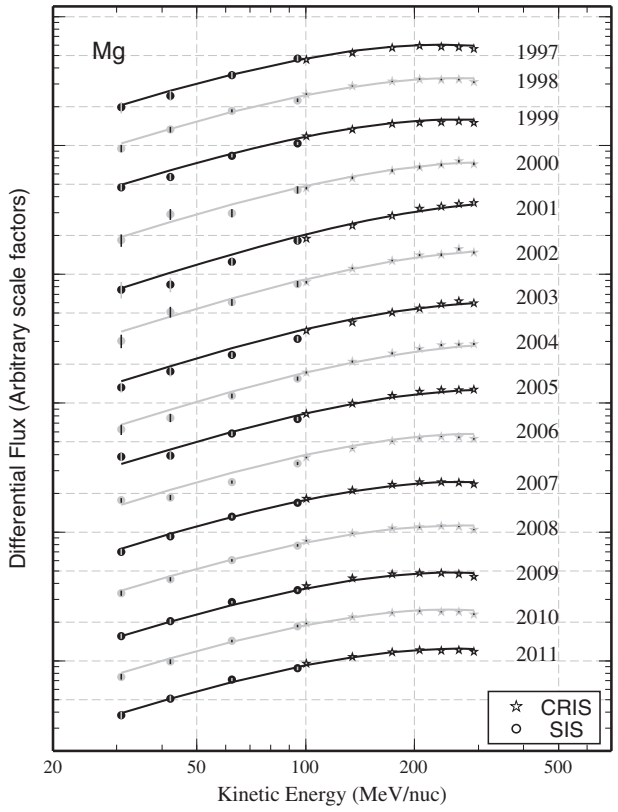

Figure 2. GCR spectra for element Mg with measurements from ACE/CRIS (stars) and ACE/SIS (circles). The solid curves show the energy spectra calculated using our model. Arbitrary scale factors have been applied to the intensity of each element for presentation of the spectral shape. Vertical bars denote the statistically standard error.

potential Φ for solar minimum and maximum. Moreover, the CRÈME96 model has also been replaced by CRÈME-MC model [*Sierawski et al.*, 2010], a physics-based model with Monte Carlo approach for simulating SEEs [*Weller et al.*, 2010].

[6] In this work we present an observation-based GCR spectra model of heavy nuclei based on the ACE/CRIS measurements over the period from 1997 to 2011, spanning over one entire solar cycle. The article is organized as follows. First, the spectra and integral intensity measurements from ACE/CRIS and ACE/SIS are presented. Then, we show the details of the development of the model step by step. Finally, we discuss the model by comparing it with previous GCR environment models.

2. Observations

[7] The daily averaged fluxes (in unit of particles/(cm^2·sr·sec·MeV/nuc)) for elemental species (nuclear charge $5 \leq z \leq 28$) of the Solar Isotope Spectrometer (SIS, if available) and the Cosmic Ray Isotope Spectrometer (CRIS) at level 2 over the period from 1997 to 2011 were readily obtained from the ACE Science Center. CRIS covers the energy range 50–500 MeV/nuc and only record GCRs for "quiet time." SIS covers the energy range 10–100 MeV/nuc and record SEP during large solar events, and GCRs or ACRs while during solar quiet time, which provides baseline for comparison with the GCR measurements from CRIS. Together, CRIS and SIS cover the element and energy range most important for evaluating the radiation risk due to heavy ions. Both CRIS and SIS have larger geometry factors and higher mass and charge resolution than previous instruments of its kind [*Stone et al.*, 1998b, 1998c]. The data are thought to be the most statistically precise for both abundant and rare species to date. The residual systematic uncertainties in the absolute spectra measured by CRIS and SIS is conservatively estimated to be less than 10% (probably less than 5%) for both instruments [*Davis et al.*, 2001].

[8] The measurements from CRIS are pure GCRs, but that from SIS are GCRs or ACRs, which may include SEP events associated with solar activity, especially during solar maximum, thereby the yearly spectra are dominated by the large SEP events [*Mewaldt et al.*, 2007]. In this paper we get the background yearly elemental fluxes of cosmic rays from SIS by automatically removing SEP events with a thresholding method [*Goring and Nikora*, 2002] following *Qin et al.* [2012]. For more details about the despiking of SIS data, the readers are referred to the Appendix A. It is noted that some elemental SIS data below 30 MeV/nuc might be from ACR, but all the SIS data over 30 MeV/nuc are mainly from GCR [*Jokipii*, 1990; *Klecker*, 1995]. While the long-term modulation of ACR is a very important issue, in this paper we focus on the GCR modulation of heavy-ions, so for all heavy elements we only study data with energy over 30 MeV/nuc. In

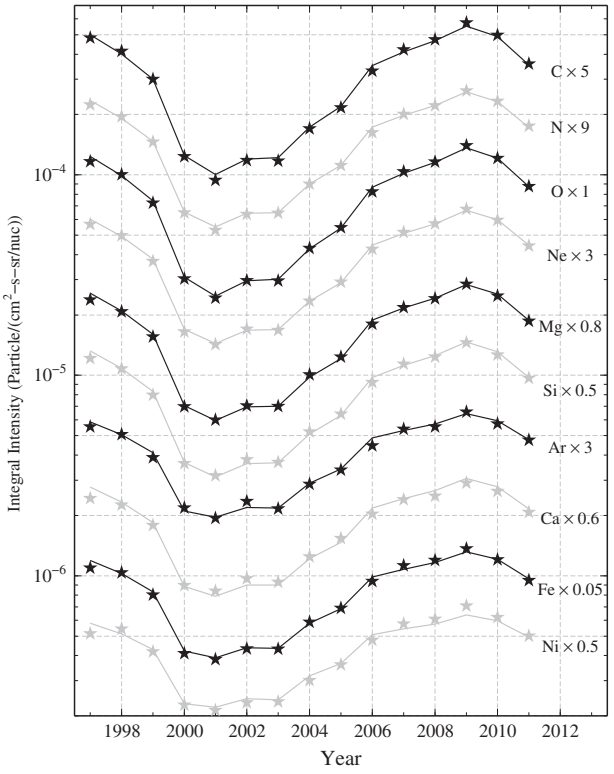

Figure 3. Integral intensity $Z(z, t)$ for several selected elements (C(6), N(7), O(8), Ne(10), Mg(12), Si(14), Ar(18), Ca(20), Fe(26), and Ni(28)) from ACE/CRIS measurements. The numbers on the right indicate the scale factors applied to the corresponding elements for presentation purpose. The solid curves represent the modeling integral intensities.

Table 1. Parameters Used in the GCR Model

Year	1997	1998	1999	2000	2001	2002	2003	2004
$\alpha(t)$	–3.91	–4.00	–4.13	–4.51	–4.61	–4.53	–4.52	–4.37
$\eta(t)$	–5.21	–5.10	–5.07	–4.36	–3.66	–3.95	–4.09	–4.01
$\bar{p}(t)$/(%)	–2.78	–1.89	–0.86	2.12	4.72	3.50	3.10	2.04
Year	2005	2006	2007	2008	2009	2010	2011	
$\alpha(t)$	–4.27	–4.06	–3.99	–3.94	–3.86	–3.92	–4.06	
$\eta(t)$	–4.40	–4.63	–4.96	–5.07	–5.20	–5.26	–5.14	
$\bar{p}(t)$/(%)	0.88	–0.70	–1.62	–2.27	–2.82	–2.39	–1.04	

z	5	6	7	8	9	10	11	12	13	14	15	16
$\bar{Z}(z)$*100	16.82	80.85	22.42	100.00	1.76	17.40	3.72	27.46	4.53	22.80	0.78	4.40
z	17	18	19	20	21	22	23	24	25	26	27	28
$\bar{Z}(z)$*100	0.89	1.97	1.58	4.32	0.96	3.52	1.70	3.47	2.21	23.80	0.15	1.25

the following, we will remove SEP spikes with our thresholding despiking method [*Qin et al.*, 2012] for all the SIS flux measurements if despiking is needed, and we refer to the despiked data as "the data" for simplicity purpose.

2.1. Energy Spectra

[9] Figure 1 shows the energy spectra during solar minimum (year 2008) and maximum (year 2002) for elemental species from boron to nickel with higher energy ACE/CRIS measurements (stars) and lower energy ACE/SIS measurements above 30 MeV/nuc (circles). In addition, Figure 2 presents the spectral shapes for element Mg from year 1997 to 2011. In both the Figures 1 and 2, dark and grey lines (symbols) alternate and arbitrary scale factors are applied to the flux of each element or each year for clear presentation of the spectral shapes. Note that not all elements available in CRIS data are available in SIS data, but those spectra in SIS data are coherently consistent with that from CRIS measurements, and they have the similar time-dependent energy spectrum shape. Therefore, in the following, we assume that all elements share the same spectral shape above $\sim$ 30 MeV/nuc, which is a function of time. Note that we fit CRIS data with a theoretical form described later in the paper, which is shown with solid lines in Figures 1 and 2.

2.2. Integral Intensity

[10] We calculate the integral intensity $I(z, t)$ by integrating the flux data with respect to energy for each element z and each year t,

$$I(z,t) = \sum_{i=1}^{N} f_i(z,t)\Delta E_i, \tag{1}$$

where $f_i(z, t)$ denotes the yearly average of differential flux observation for element z in the year t, and ΔE_i indicates the ith energy interval of the CRIS instrument. Here for the CRIS data, the number N of energy channels for each element is 7. The integral intensities are measured over different energy ranges for different elements, due to the z dependence of the energy coverage of the CRIS instrument. Therefore, the integral intensity is just an analogue of abundance, and it cannot be directly compared with abundance derived using a fixed energy interval for all elements, as is conventionally done [*George et al.*, 2009].

[11] Figure 3 shows the time variation of integral intensities for several selected elements, including C, N, O, Ne, Mg, Si, Ar, Ca, Fe, and Ni, from the year 1997 to 2011. It is noted that the integral intensities of all elements approximately show the similar variation pattern, which exhibit apparent anti-correlation with solar activity. In particular, the integral intensities during the solar minimum (1997, 2009) are higher than that during the solar maximum (2001) by a factor of $\sim$ 5. It is also shown that the integral intensities in the solar minimum of the year 2009 are approximately 20% greater than that in the solar minimum of the period 1997–1998 due to the extremely low solar activity during the prolonged solar minimum [see also, *Mewaldt et al.*, 2010].

3. Spectra Model

[12] The model construction generally involves two procedures. First, an integral intensity model is developed to characterize the element-dependent and time-dependent integral intensity. Then, an appropriate form is used to fit the spectral shapes of all elements. Combining the two together, we get the final energy spectra model.

3.1. Integral Intensity Model

[13] In the following we construct an integral intensity model by calculating the intensity ratio $Z(z, t)$ and the intensity modulation parameter $\alpha(t)$.

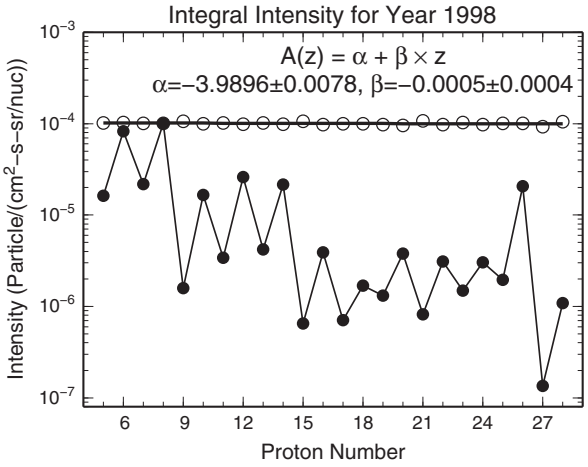

Figure 4. An example of estimation of intensity modulation parameter $\alpha(t)$ in 1998. The filled circles show the intensity $I(z, t)$ from ACE/CRIS measurements, while the open circles show the corrected intensity $I^c(z, t)$, which is then fitted by a straight line in log-linear plot. The slope is approximately zero, and the intercept is defined as the intensity modulation parameter α.

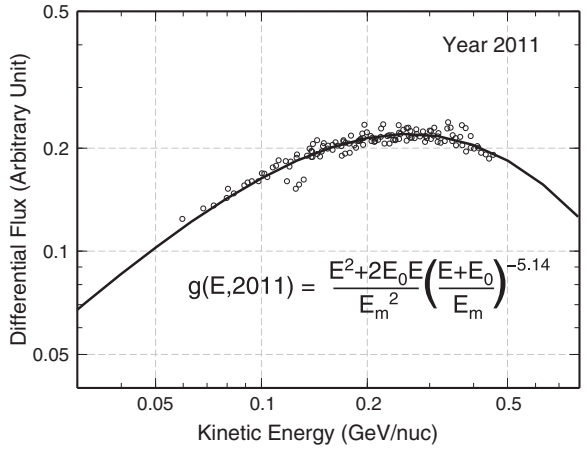

Figure 5. Fitted spectral shape for the year 2011. Circles indicate ACE/CRIS measurements, which are multiplied by a free parameter for each element and each year.

[14] *George et al.* [2009] showed that, similar to the solar system abundances, the elemental GCR abundances of heavy-ions present an odd-even law. In addition, the abundances of different elements can vary over three orders of magnitude. In order to characterize the relative integral intensity of each element, we first calculate the intensity ratio of each element with respect to O(8). As in many previous studies [e.g., *Mason et al.*, 1997, 2008], we choose O as the reference element for its high abundance. Here, we define the intensity ratio $Z(z, t)$ with respect to O(8) as

$$Z(z,t) = \frac{I(z,t)}{I(z=8,t)}. \tag{2}$$

With some procedures we can get the intensity ratio model $Z^m(z, t)$ as

$$Z^m(z,t) = \bar{Z}(z)\left(1 + \frac{\lambda(z)\bar{p}(t)}{\sqrt{\bar{Z}(z)}}\right), \tag{3}$$

where $\bar{Z}(z)$ and $\bar{p}(t)$ denote the averaged intensity ratio and averaged intensity ratio percentage, respectively, and $\lambda(z = 6) = 0$, $\lambda(z = 8) = 0$, $\lambda(z = 26) = 3.3$, and $\lambda(z) = 1$ otherwise. The values of $\bar{Z}(z)$, and $\bar{p}(t)$ are shown in Table 1. The reader can refer to Appendix B for the details of the derivation of intensity ratio model $Z^m(z, t)$.

[15] It is shown that the integral intensity of each element varies with time, or with the variation of solar modulation strength. So a successful GCR modulation model should reflect such process with some modulation parameters. The solar modulation potential Φ is widely used in GCR models. Here we characterize the solar modulation process with an intensity modulation parameter α, which relates the varying integral intensity of heavy ions to the solar activity.

[16] Figure 4 shows an example of intensity modulation parameter α estimation for the year 1998. First, the corrected integral intensities $I^c(z, t)$ are calculated with equation (4).

$$I^c(z,t) = I(z,t)/Z^m(z,t) \tag{4}$$

Then, the corrected integral intensity is fitted using a straight line in the log space. From Figure 4 we can see that the fitted line is

$$\lg[I^c(z, t = 1998)] \approx \alpha + \beta z, \tag{5}$$

with $\alpha = -3.9896 \pm 0.0078$ and $\beta = -0.0005 \pm 0.0004$, or the slope of the fitted line is approximately zero for the year 1998, i.e., $I^c(z, t = 1998) \approx 10^{\alpha}$ with $\alpha(t = 1998) \approx -3.99$.

[17] Furthermore, we apply the same procedure to the integral intensities of the other years to get similar results

Table 2. Measurement Energy Intervals of ACE/CRIS Downloaded From ACE Home Page (http://www.srl.caltech.edu/ACE/ASC/)[a]

Element	E_1	ΔE_1	E_2	ΔE_2	E_3	ΔE_3	E_4	ΔE_4	E_5	ΔE_5	E_6	ΔE_6	E_7	ΔE_7
B(5)	59.6	14.4	79.7	23.1	102.0	19.1	121.1	16.8	138.3	15.3	154.0	14.1	168.6	13.5
C(6)	68.3	16.6	91.4	26.6	117.2	22.1	139.2	19.5	159.1	17.8	177.3	16.4	194.4	15.7
N(7)	73.2	17.8	98.1	28.5	125.8	23.8	149.5	21.0	171.0	19.2	190.6	17.7	209.1	16.9
O(8)	80.4	19.6	107.8	31.5	138.4	26.3	164.7	23.3	188.4	21.3	210.2	19.7	230.7	18.8
F(9)	83.5	20.4	112.0	32.8	143.8	27.4	171.1	24.3	195.9	22.2	218.7	20.6	240.0	19.6
Ne(10)	89.4	21.8	120.0	35.2	154.3	29.5	183.8	26.1	210.5	24.0	235.1	22.2	258.2	21.2
Na(11)	94.0	23.1	126.2	37.1	162.3	31.2	193.5	27.6	221.7	25.4	247.8	23.5	272.3	22.6
Mg(12)	100.2	24.6	134.6	39.8	173.3	33.3	206.7	29.6	237.0	27.3	265.0	25.4	291.4	24.2
Al(13)	103.8	25.6	139.6	41.3	179.8	34.7	214.6	30.9	246.1	28.4	275.3	26.4	302.8	25.2
Si(14)	110.0	27.1	148.2	44.0	191.0	37.0	228.1	33.0	261.8	30.4	293.1	28.3	322.5	27.1
P(15)	112.7	27.8	151.8	45.1	195.8	38.0	233.9	33.9	268.7	31.2	300.8	29.1	331.1	27.9
S(16)	118.2	29.2	159.3	47.4	205.6	40.1	245.8	35.8	282.4	32.9	316.4	30.7	348.5	29.5
Cl(17)	120.0	29.8	161.8	48.2	209.0	40.8	249.9	36.4	287.2	33.6	321.8	31.4	354.5	30.1
Ar(18)	125.1	31.1	168.9	50.5	218.2	42.7	261.1	38.2	300.3	35.3	336.6	32.9	371.0	31.7
K(19)	127.9	31.9	172.7	51.7	223.3	43.9	267.3	39.2	307.5	36.3	344.8	33.9	380.2	32.5
Ca(20)	131.7	32.8	178.1	53.5	230.3	45.3	275.9	40.5	317.5	37.5	356.2	35.1	392.9	33.8
Sc(21)	133.5	33.4	180.5	54.4	233.6	46.0	279.9	41.2	322.2	38.1	361.5	35.7	398.8	34.4
Ti(22)	137.1	34.3	185.5	55.9	240.1	47.5	287.9	42.5	331.5	39.4	372.2	36.9	410.7	35.5
V(23)	139.9	35.1	189.4	57.2	245.4	48.6	294.3	43.6	339.1	40.4	380.7	37.9	420.3	36.4
Cr(24)	143.9	36.1	194.9	59.0	252.7	50.2	303.1	45.0	349.4	41.8	392.6	39.1	433.5	37.8
Mn(25)	146.8	37.0	199.0	60.3	258.1	51.3	309.7	46.2	357.2	42.8	401.4	40.2	443.4	38.7
Fe(26)	150.5	37.9	204.1	62.1	264.9	52.8	318.1	47.5	367.0	44.1	412.6	41.4	455.9	39.9
Co(27)	153.5	38.9	208.4	63.4	270.6	54.1	325.1	48.7	375.2	45.2	422.0	42.5	466.5	41.1
Ni(28)	159.0	40.2	216.0	66.0	280.7	56.4	337.5	50.8	389.7	47.1	438.5	44.4	485.0	42.9

[a] E_i indicates the recommended midpoint of each energy range, and ΔE_i is the corresponding energy interval. All energies have a unit of MeV/nuc.

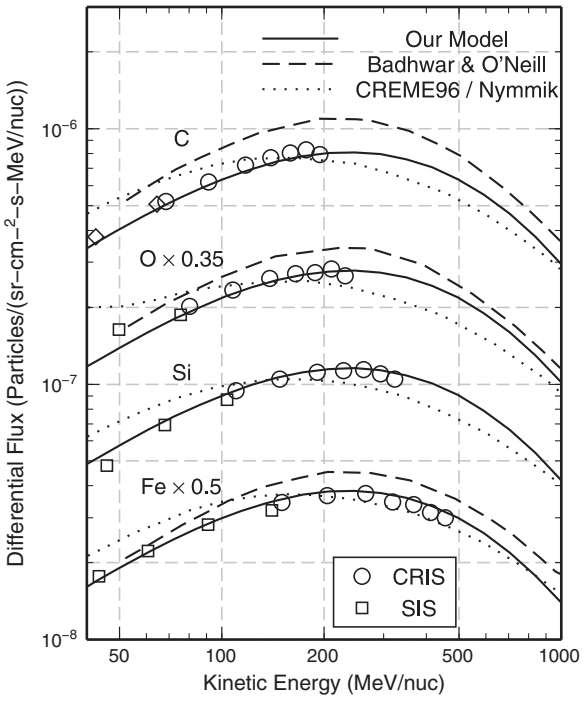

Figure 6. Comparison between energy spectra from CRÈME96/Nymmik model (dotted line), and Badhwar and O'Neill model (dashed line), which are digitized from *Davis et al*. [2001, Figure 4] and that from our model (solid line), for elements C, O, Si, and Fe in 1997. Note that the energy spectra of Si for Badhwar and O'Neill model is missing. In addition, the ACE/CRIS (circles) and SIS (squares) measurements for the elements studied during September 1997 to March 1998 are also shown.

with different $\alpha(t)$, i.e., $I^c(z,t) \approx 10^{\alpha(t)}$. The variation of α with time t is shown in Table 1.

[18] After getting the above parameters, the integral intensity model can be expressed as equation (6). So we can get the estimation of integral intensity over the energy interval of CRIS measurement for any element z from 5 to 28 and any year t from 1997 to 2011.

$$I^m(z,t) = Z^m(z,t)10^{\alpha(t)} \tag{6}$$

[19] In order to evaluate the integral intensity model, we compare the modelling intensities $I^m(z,t)$ with the observations $I(z,t)$. The solid curves in Figure 3 represent the modelling results, while the filled stars indicate the observations. It can be seen that the modeling results agree quite well with the observations for all elements ($5 \le z \le 28$) and all years ($1997 \le t \le 2011$). To further validate the integral intensity model, we compute the misfit $E(t)$ with equation (7)

$$E(t) = \frac{1}{24}\sum_{Z=5}^{28}\left|\frac{I^m(z,t) - I(z,t)}{I(z,t)}\right| \times 100\%, \tag{7}$$

We find that the misfit for all years are within 5% except for the year 1997 that is approximately 10%, which indicates the integral intensity model is generally acceptable.

3.2. Spectral Shape Function

[20] Generally, the spectra of all elements share the same shape in the same year (Figure 1). In addition, the spectral shape may change under different solar modulation strength, e.g., the spectra for solar maximum is slightly different from that for solar minimum (Figure 2). Therefore, it is reasonable to assume that all elements share the same spectral shape which varies gradually over different years, and we can fit the spectral shape with an appropriate formula.

[21] It is essential to decide with what kind of spectral shape to fit observational data. *Zhang* [1999] used the following model to describe the interstellar GCR proton spectrum,

$$j_{ism}(p) \propto \left(m_0^2c^2 + p^2\right)^{-1.8} p. \tag{8}$$

After testing with the ACE/CRIS data, we adopt a similar format to fit the energy spectrum shape of elemental GCR in the solar wind

$$g(E,t) = \frac{E^2 + 2E_0E}{E_m^2}\left(\frac{E+E_0}{E_m}\right)^{\eta(t)}, \tag{9}$$

where E is the kinetic energy per nucleon for any heavy ion of the year t, E_m = 1 GeV, E_0 is the rest energy of proton, and $\eta(t)$ is a parameter as a function of the year t.

[22] In order to get the spectral shape $g(E,t)$, we have to obtain the parameter $\eta(t)$ for each year by fitting the ACE/CRIS data with the equation (9). For each year and element, we multiply the flux from ACE/CRIS measurement by a free parameter to get the best fit of the model shown in the equation (9). Figure 5 shows an example to fit the ACE/CRIS

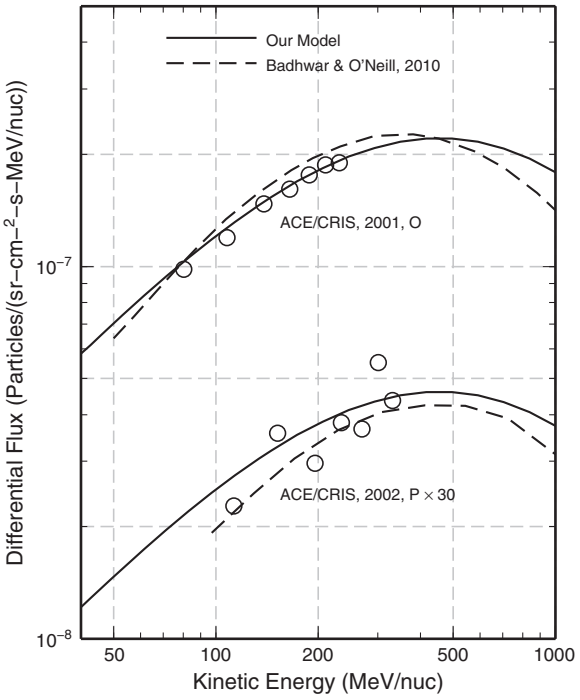

Figure 7. Comparison between energy spectra from Badhwar & O'Neill 2010 model (dotted line, digitized from *O'Neill* [2010, Figures 3 and 4] and that from our model (solid line) for O (abundant element) and P (rare element). In addition, the ACE/CRIS (circles) measurements are also shown.

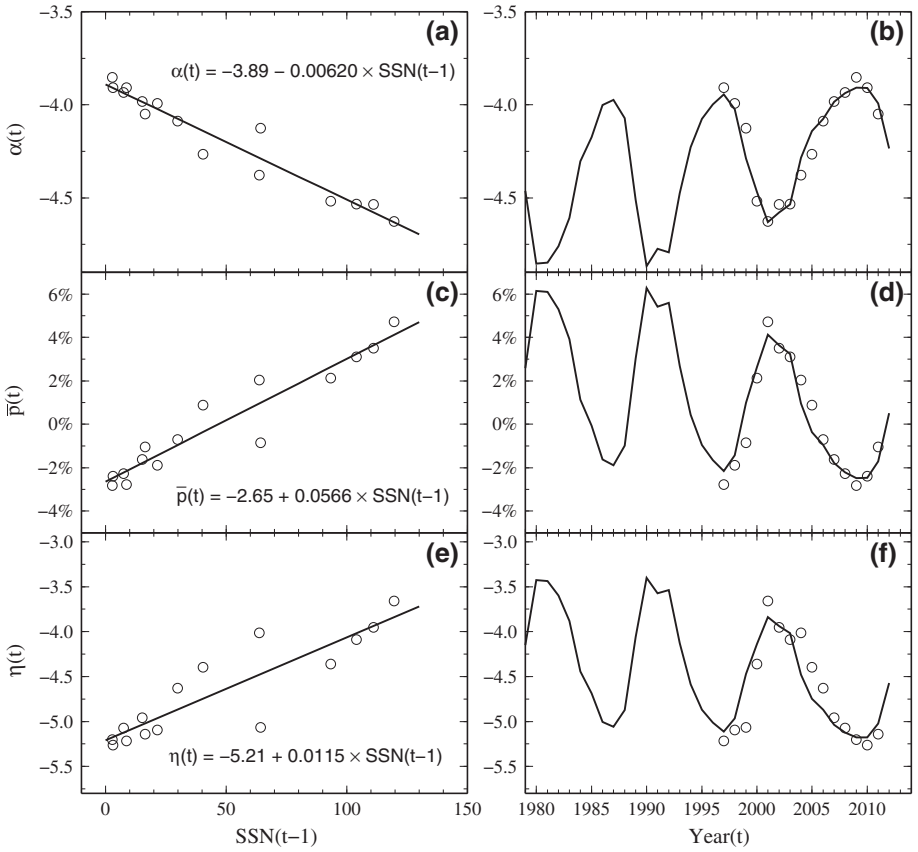

Figure 8. Intensity modulation parameter $\alpha(t)$, averaged IRP $\bar{p}(t)$, and spectral shape function parameter $\eta(t)$ by fitting ACE/CRIS measurements to our spectra model (circles). (a, c, and e) show the parameters varied with sunspot numbers of the previous year, SSN(t–1), while (b, d and f) show the parameters varied with year(t). Solid lines in Figures 8a, 8c and 8e indicate linear fitting of the parameters to SSN(t–1), from which the parameters are estimated with SSN over the last three solar cycles shown with solid curves in Figures 8b, 8d and 8f.

data with the spectral shape for the year 2011, and the best $\eta(t = 2011)$ we get is –5.14. For each year of 1997–2011, we fit the spectral shape to get the best $\eta(t)$, which are shown in the Table 1.

3.3. Final Energy Spectra Model

[23] With all the above procedures, we can finally write the energy spectra model for any element z, year t, and kinetic energy per nucleon E as

$$f(z,t,E) = I^m(z,t)N(z,t)g(E,t) = Z^m(z,t)10^{\alpha(t)}N(z,t)g(E,t) \quad (10)$$

where $N(z,t)$ indicates a normalize factor function, which can be obtained using the equation (11)

$$N(z,t) = \left(\sum_{i=1}^{7} g(E_i,t)\Delta E_i\right)^{-1} \quad (11)$$

[24] We show the results from this model for all elements for both solar minimum (year 2002) and maximum (year 2008) with solid curves in Figure 1, which agree remarkably well with the ACE/CRIS observations (stars in Figure 1) for most elements. Even though the spectra model is deduced from the data sets of CRIS, we can extend the modeling results to lower energy with extrapolation. Surprisingly, the extended spectra still agree quite well with measurements from SIS at lower energy (circles in Figure 1) for most GCR elements, e.g., elements Na, Mg, Al, Si, and Fe.

[25] Furthermore, we show the comparison between the modeling results and observations from both CRIS and SIS for element Mg(12) in the energy range from 30 to 350 MeV/nuc over the period 1997–2011 in Figure 2. The modeling results agree well with the observations, especially during the solar minimum.

[26] Table 1 shows the parameters $\alpha(t)$, $\eta(t)$, $\bar{p}(t)$, and $\bar{Z}(z)$ used in our elemental GCR model. In addition, Table 2 shows the measurement energy intervals of ACE/CRIS downloaded from ACE Home page (http://www.srl.caltech.edu/ACE/ASC/) used in equations (1) and (11), where E_i indicates the recommended midpoint of each energy range and ΔE_i is the corresponding energy interval. All energy has a unit of MeV/nuc.

[27] In order to compare our model with the others, in Figure 6, we show results from CRÈME96/Nymmik model (dotted line) and Badhwar and O'Neill model (dashed line), which are digitized from *Davis et al*. [2001, Figure 4] as well as that from our model, for elements C, O, Si, and Fe for the year 1997. In addition, following *Davis et al.* [2001], we show the ACE/CRIS (circles) and SIS (squares) measurements for the elements studied during Sept. 1997 to March 1998. From the figure, we can see for the

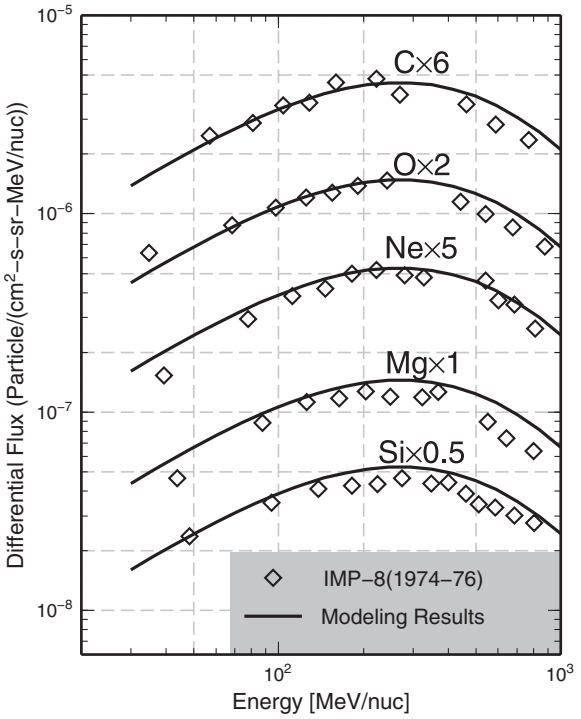

Figure 9. Energy spectra for C(6), O(8), Ne(10), Mg(12) and Si(14) during 1974–1976. Diamonds indicate the observed spectra by IMP-8 spacecraft [digitized from *Garcia-Munoz et al.*, 1977], and solid curves indicate the average of modeling spectra for the years 1974–1976 using our spectra model with extrapolated parameters.

elements, time period and energy range studied, that our model reproduces ACE observations better than the other two models.

[28] Recently, Badhwar and O'Neill model is revised based on the newer ACE measurements and could be named as Badhwar and O'Neill 2010 model [*O'Neill*, 2010]. Figure 7 shows comparison between energy spectra from Badhwar and O'Neill 2010 model, which is digitized from *O'Neill* [2010, Figures 3 and 4] (dotted line) and that from our model (solid line) for O (abundant element) and P (rare element). In addition, the ACE/CRIS (circles) measurements are also shown. From the figure, we can see that both of the models do not agree with ACE measurements for P (rare element) very well due to the data's low statistics. But for O (abundant element), the Badhwar and O'Neill 2010 model is improved compared to the original Badhwar and O'Neill model, and both the models Badhwar and O'Neill 2010 model and our model agree with ACE/CRIS measurements very well. However, our model still shows better performance than the Badhwar and O'Neill 2010 model.

3.4. Prediction of GCR

[29] A successful GCR spectra model should characterize the time-variation of GCR flux. The Badhwar and O'Neill model and the CRÈME96/Nymmik model achieve the goal through different approaches. Our model is similar to CRÈME96/Nymmik model in the approach.

[30] As shown in Figure 8, the intensity modulation parameter $\alpha(t)$, averaged intensity ratio percentage $\bar{p}(t)$ (see Appendix B for detail), and energy spectra parameter $\eta(t)$ exhibit strong correlation with solar activity. Similar to the CRÈME96/Nymmik model, we directly relate the three parameters, $\alpha(t)$, $\bar{p}(t)$, and $\eta(t)$ to the sunspot number (SSN), and reconstruct the parameters with continuous SSN record. However, the correlation between the SSN and the GCR intensity at near-Earth environment is not simple, e.g., there is a time-lag between the SSN and GCR intensity level near Earth, since it takes time for the dynamic solar wind plasma and the embedded interplanetary magnetic field to propagate to the boundary of the heliosphere. *Badhwar and O'Neill* [1993] suggested the time delay is about 270 days (10 Bartel Rotation period), but *Tylka et al.* [1997] assumed the time delay is approximately 1 year. However, *Nymmik and Suslov* [1995] showed that the time lag is rigidity-dependent and varies during the odd and even solar cycles. In our case, we follow the CRÈME96/Nymmik model and take the time lag as 1 year for simplicity. We have also tried other proxies of solar activity, e.g., counts rates from neutron monitor (NM) with various cutoff rigidities. However, as mentioned above, the NM count rates are sensitive to the reaction products of higher energy cosmic rays (1–20 GeV), and may underestimate the lower energy part of the GCR spectra [*Usoskin et al.*, 2011]. Generally, the SSN shows superior performance for our case. Even so, we should bear in mind that we do not have a way to predict the proxies reliably in the future.

[31] In Figures 8a, 8c and 8e, we study $\alpha(t)$, $\bar{p}(t)$, and $\eta(t)$ varied with sunspot numbers of the previous year, SSN(t–1).

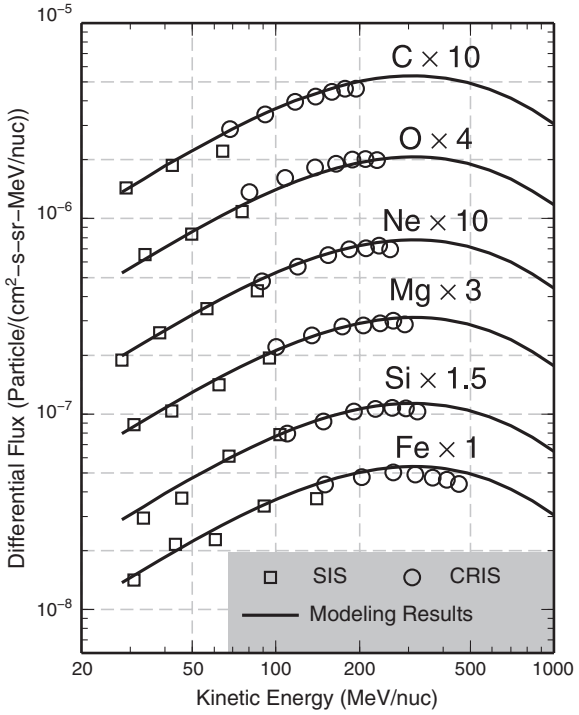

Figure 10. Energy spectra of C(6), O(8), Ne(10), Mg(12), Si(14) and Fe(26) for the year 2012. Open squares and circles denote the observed spectra from SIS and CRIS, respectively. Solid curves indicate the modeling spectra using our spectra model with extrapolated parameters.

In Figures 8b, 8d and 8f, we show the same parameters varied with time t. From Figure 8a, we can see that the intensity modulation parameter $\alpha(t)$ shows strong anti-correlation with sunspot numbers of the previous year, SSN($t-1$), and the linear fitting of the $\alpha(t)$ to SSN($t-1$) as

$$\alpha(t) = -3.89 - 0.00620 \times SSN(t-1). \quad (12)$$

Using the regression line equation (12) and the SSN records, we reconstruct the intensity modulation parameter $\alpha(t)$ for the last three solar cycles (1980–present) (solid line in Figure 8b). Similar to the intensity modulation parameter, the average intensity ratio percentage ($\bar{p}(t)$) (Figure 8c) and the energy spectra parameter $\eta(t)$ (Figure 8e) exhibit positive linear correlation with SSN, so $\bar{p}(t)$ and $\eta(t)$ can be linearly fit as

$$\bar{p}(t) = -2.65 - 0.0566 \times SSN(t-1), \quad (13)$$

and

$$\eta(t) = -5.21 + 0.0115 \times SSN(t-1), \quad (14)$$

respectively. Furthermore, we use the regression line equations (13) and (14) and the SSN records to reconstruct the $\bar{p}(t)$ and $\eta(t)$ for the last three solar cycles shown with solid lines in Figures 8d and 8f, respectively. We also show the parameters $\alpha(t)$, $\bar{p}(t)$, and $\eta(t)$ fit from ACE/CRIS data during 1997–2011 as circles in Figure 8. From Figures 8a, 8c and 8e, we can see, the parameters reconstructed using regression line equations and SSN records (solid lines) agree very well with the ones fit from ACE/CRIS data (circles).

[32] To further validate our model, previous observations were compared with the prediction of our model. The GCR flux of several elements, including C, O, Ne, Mg and Si, were measured by IMP-8 spacecraft during 1974–1976 [*Garcia-Munoz et al.*, 1977]. These data represented the best available solar minimum heavy-ion spectra in the energy range 50–1000 MeV/nuc [*Davis et al.*, 2001]. Unfortunately, the heavy-ion spectra from IMP-8 for other time periods have not been published to the best of our knowledge. Using the reconstructed parameters, we reproduce the GCR fluxes for the years 1974–1976 for the five elements using our spectra model, from which we get the average fluxes for the period 1974–1976, which fit the observations quite well within the studied energy range (Figure 9). It is thus suggested that our model can reproduce the heavy-ion spectra in the past with reasonable accuracy. Hence, we expect that our model can also produce reliable spectra prediction for the year 2012 using SSN of the year 2011. At the time this manuscript is prepared, we can access the GCR measurement from ACE spacecraft for the first 11 months of the year 2012. Figure 10 presents the spectra comparison of element C(6), O(8), Ne(10), Mg(12), Si(14) and Fe(26) between the observations and modeling results. It is shown that the spectra using our model agree remarkably well with the observations. Of course, more elemental GCR spectra of heavy nuclei in the future are needed to further validate our model. The ACE spacecraft is scheduled to remain operational until 2014, so we can continue to use the GCR spectra observations from ACE spacecraft for the modeling test.

4. Conclusion and Discussion

[33] In this paper, we present an ACE/CRIS-observation-based elemental GCR spectra model. Our model is entirely characterized by four parameters, including the averaged intensity ratio $\bar{Z}(z)$ and the averaged intensity ratio percentage (IRP) $\bar{p}(t)$, which represents the relative intensity of each element, intensity modulation parameter $\alpha(t)$, which relates the varying GCR intensity to the solar activity, and the spectral shape function parameter $\eta(t)$, which describes the GCR energy spectra depending on the solar activity. Although the model seems to be too simple compared with the previous comprehensive GCR models, e.g., ACR and SEP models are included in CRÈME96/Nymmik model primarily based on the SAMPEX results [*Tylka et al.*, 1997], our model gives reasonably accurate fits to the ACE/CRIS measurements of GCR, with misfit less than 5%, and the modeling results are also in good agreement with the GCR spectra from ACE/SIS measurements for the near-earth radiation environment, especially during the solar minimum. So it is claimed that our model can give adequately accurate energy spectra of heavy nuclei and that it is useful, e.g., for manned space mission in understanding the near-earth radiation environment within the energy range 30–500 MeV/nuc. Additionally, the comparison between the modeling results and observations from both ACE and IMP-8 spacecraft demonstrates the reliability of our model.

[34] Compared with previous elemental GCR models, the spectra model we present has some features as follows. First, our model is based on highly statistically precise data from ACE/CRIS, so it provides improved fitting to the ACE measurements. Therefore, there exist less statistical and systematic uncertainties. Second, our model is an empirical and phenomenological one, which is derived completely from observations, without consideration of the physical process such as diffusion and convection for GCR's propagating through the heliosphere, so it is more straightforward and applicable in practice. Note that *Paouris et al.* [2012] provides a GCR modulation model using a series of solar activity indices and heliospheric parameters, such as sunspot number, interplanetary magnetic field, coronal mass ejections index, heliospheric current sheet, monthly flares number, geomagnetic index, flare index, and number of CMEs, etc. However, we only use the sunspot number for predicting the parameters in our model. Relatively speaking, our model is simpler and more convenient. In fact, since our model is very simple and all of its parameters are shown, our model can be easily coded by following this article.

[35] In this work, we make two assumptions for simplicity purpose, which may be violated in practice, so the inaccuracy could be introduced. First, we assume that all elements share the same spectral shape that is only a variable of time. However, this assumption is not accurate for representing the spectra of all elements, since the spectra of the abundant elements are different from that of the rare species. However, we can still claim that the assumption is good enough in the energy range studied, especially for the relative abundant elements which contribute mostly to the radiation hazard. Furthermore, we assume that the intensity ratio percentage (IRP) for all the elements are generally the same, except C(6), O(8) and Fe(26). However, it is shown that the assumption is approximately valid for ACE/CRIS measurements (see Appendix B).

[36] In order to evaluate our model, it is necessary for us to compare our results with that of the previous models that are widely used. However, it is not easy for us to

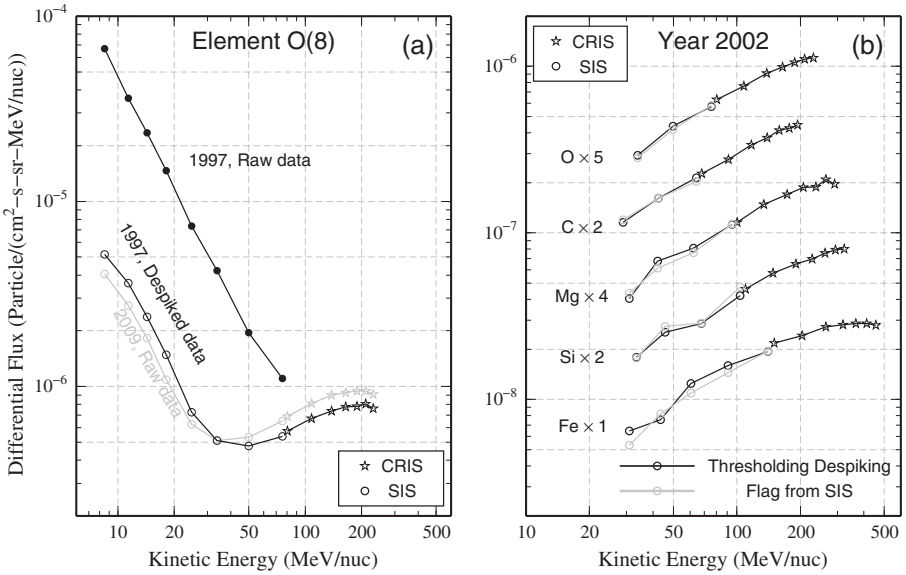

Figure A1. (a) Comparison of O spectra between raw and despiked data. Stars and circles denote ACE/CRIS and ACE/SIS data, respectively, with open symbols for raw data and filled symbols for despiked data. Flux data of the year 1997 and that of the year 2009 are shown with dark and grey symbols, respectively. (b) Comparison of spectra of elements between despiked data with flag obtained with our method [*Qin et al.*, 2012] denoted as "Thresholding Despiking", and that with the solar activity flag provided by SIS data denoted as "Flag from SIS". The symbols are similar to Figure A1a, except that the grey ones indicate the data despiked with "Flag from SIS".

code those models independently by just following the literatures; here we only obtain the results of some models by digitizing figures in literatures, so we only make some preliminary comparison between our model and other ones. In the future, we would collect more data sets to further validate our model. Moreover, we need to compare our model with previous ones much more completely.

Appendix A: Despiking of Flux Data

[37] Recently, based on the Poincare map thresholding method [*Goring and Nikora*, 2002], *Qin et al.* [2012] used a robust automatic despiking algorithm to "purify" the time-series GCR fluxes from spacecraft observations. In this work, with the same despiking algorithm as in *Qin et al.* [2012], we use O(8) data of SIS measurements to flag periods of spikes, potentially caused by SEP events. Therefore, we can get the background yearly elemental fluxes of heavy nuclei of SIS measurements by getting rid of the flag periods of data contaminated by SEPs. Figure A1a shows the comparison of energy spectra for O(8) of the year 1997 (dark) and 2009 (grey). Since in the year 2009 all the elemental fluxes of SIS data contain much fewer spikes due to the prolonged solar minimum and are dominated by the background GCR or ACR component, they have the same values after the despiking, so here we only show the raw data from SIS. It is shown that in the year 1997 the raw data spectrum at lower energy (SIS data points) have a form of power-law with negative spectral index $\sim$ –2, and after despiking, it is reduced to a much lower level to closely track the raw data of the year 2009.

[38] We also note that the data from SIS instrument include a "solar activity flag" that flags periods with significant SEP contributions, and we can calculate the yearly averaged fluxes by getting rid of the periods of data with such flag. Figure A1b illustrates the energy spectra of year 2002 for several elements (including O, C, Mg, Si, and Fe) from CRIS and SIS instruments. The SIS data are despiked in two different ways. The first way is to despike the data with flag obtained with our method [*Qin et al.*, 2012] denoted as "Thresholding Despiking", and the second one is to despike the data with the solar activity flag provided by SIS data denoted as "Flag from SIS" in Figure A1b. It is shown that the spectra from the two methods are almost identical, above 30 MeV/nuc, even during the solar maximum dominated by SEP events, which validates our despiking method [*Qin et al.*, 2012]. Especially, our despiking method could be helpful for other spacecraft data when such a solar activity flag is not provided.

Appendix B: Intensity Ratio

[39] The intensity ratio characterizes the relative intensity of each element. The construction of the intensity ratio is introduced briefly here.

[40] The intensity ratio is defined as equation (2), and averaged intensity ratio $\bar{Z}(z)$ as

$$\bar{Z}(z) = \frac{1}{15}\sum_{t=1997}^{2011} Z(z,t). \tag{B1}$$

[41] As an example, Figure B1a shows the intensity ratio of Si with respect to O. It is shown that the intensity ratio $Z(z = 14, t)$, with averaged value $\bar{Z}(z = 14) \sim 0.23$, varies from 0.21 to 0.26 with time and exhibits positive correlation with the solar activity. *Mason et al.* [1997] found the similar results that the abundance ratio of any element with respect to O (e.g., C/O, Mg/O, or Fe/O) depends on solar wind speed

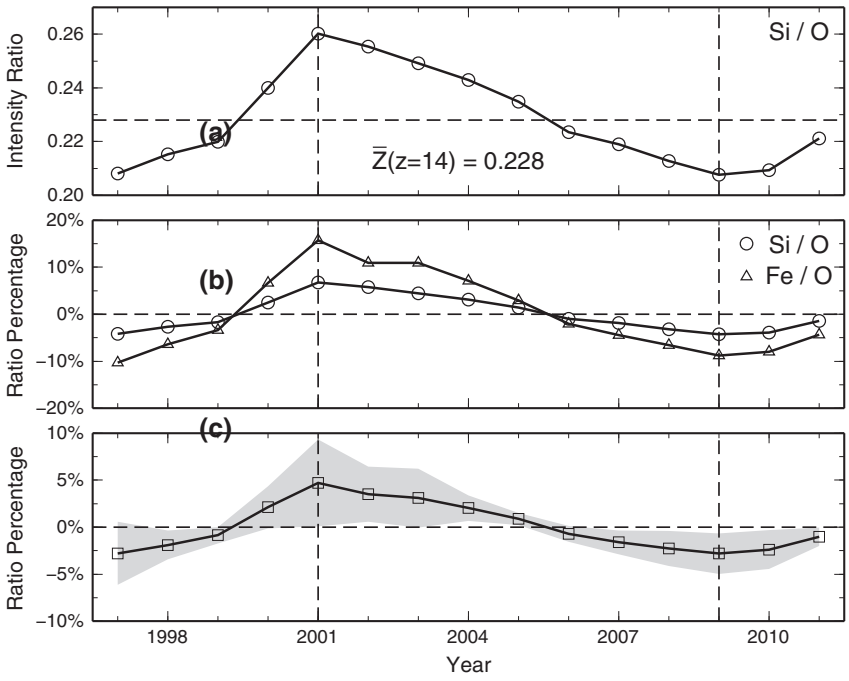

Figure B1. (a) The intensity ratio for element Si with respect to O, $Z(z = 14, t)$. (b) The intensity ratio percentage(IRP) for Si, $p(z = 14, t)$ and that for Fe, $p(z = 26, t)$ shown with circles and triangles, respectively. (c) The averaged IRP $\bar{p}(t)$. The grey shadow indicates the $\pm\delta$ statistically standard error.

and essentially correlates with solar activity. The intensity ratio of the majority elements also exhibit the similar variation pattern. Figure B2 shows the averaged intensity ratio $\bar{Z}(z)$ for elements ($5 \leq z \leq 28$). It is shown that $\bar{Z}(z)$ generally share similar characteristics with the common elemental abundances of GCR, e.g., odd-even law and Fe-peak. It is noted that for O(8), $Z(z = 8, t) = \bar{Z}(z = 8) = 1$. We also show $\bar{Z}(z)$ in Table 1.

[42] Since the intensity ratio $Z(z, t)$ varies with time, with a variation amplitude depending on the averaged ratio $\bar{Z}(z)$, we define the intensity ratio percentage (IRP)

$$p(z,t) = \frac{Z(z,t) - \bar{Z}(z)}{\sqrt{\bar{Z}(z)}} \times 100\%. \tag{B2}$$

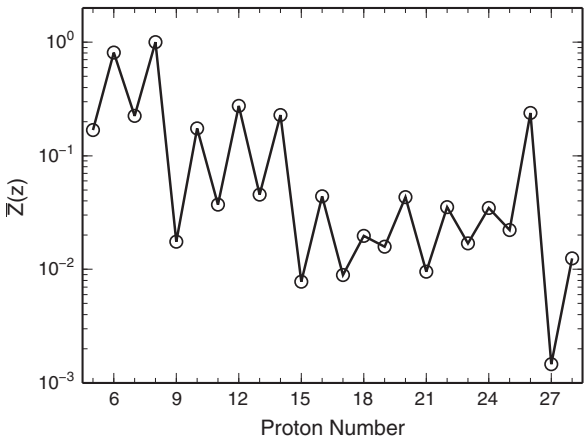

Figure B2. The averaged intensity ratio $\bar{Z}(z)$ for elements from boron to nickel.

Although different elements have different ratio variation amplitudes, the IRP of any certain year are nearly identical for the majority of the elements (except C, O and Fe). Figure B1b shows the intensity ratio percentage (IRP) varied with time for Si (circles, one of normal elements) and Fe (triangles). We can see that the IRP for both Fe and Si are correlated strongly with solar activity, the only difference is that the variation amplitude of IRP for Fe is approximately three times larger. In addition, the IRP of C (not shown) varies irregularly and approximately remains zero, thus the IRP of C(6) is set to zero for this model, i.e., $p(z = 6, t) = 0$. In addition, for O(8), since $Z(z = 8, t) = \bar{Z}(z) = 1$, the IRP of O(8) is also zero. Furthermore, we average the IRPs over all elements (except C, O and Fe) for each year to obtain $\bar{p}(t)$ shown in Figure B1c and Table 1. The grey shadow indicates the $\pm\delta$ statistical error. It is shown that the IRP varies within $\pm 5\%$ for normal elements. In addition, the averaged ratio between $p(z = 26, t)$ and $\bar{p}(t)$ is 3.3. Based on the above analysis, we make the second assumption in our model that the IRP for all the elements (except C(6), O(8) and Fe(26)) can be replaced with its average, which correlates strongly with solar activity. Furthermore, from equations (B2) we can get

$$Z(z,t) = \bar{Z}(z)\left(1 + \frac{p(z,t)}{\sqrt{\bar{Z}(z)}}\right). \tag{B3}$$

[43] This way, we get the intensity ratio model $Z^m(z, t)$ for elements $5 \leq z \leq 28$ as

$$Z^m(z,t) = \bar{Z}(z)\left(1 + \frac{\lambda(z)\bar{p}(t)}{\sqrt{\bar{Z}(z)}}\right), \tag{B4}$$

where $\lambda(z = 6) = 0$, $\lambda(z = 8) = 0$, $\lambda(z = 28) = 3.3$, and $\lambda(z) = 1$ otherwise.

[44] **Acknowledgments.** We are partly supported by grants NNSFC 41074125, NNSFC 41125016, CMA grant GYHY201106011, and the Specialized Research Fund for State Key Laboratories of China. The data sets of SIS and CRIS are downloaded from the ACE Science Center archives at http://www.srl.caltech.edu/ACE/ASC/level2/. We also acknowledge the use of the sunspot number data provided to the community by NASA.

References

Badhwar, G. D., and P. M. O'Neill (1993), Time lag of twenty two year solar modulation, in *Proc. 23rd Int. Cosmic Ray Conf. (Calgary)*, vol. 3, pp. 535–538, Dept. Phys. Astron., Univ. of Calgary, Calgary, Can.

Badhwar, G. D., and P. M. O'Neill (1994), Long-term modulation of galactic cosmic radiation and its model for space exploration, *Adv. Space. Res.*, *14*(10), 749–757, doi:10.1016/0273-1177(94)90537-1.

Badhwar, G. D., and P. M. O'Neill (1996), Galactic cosmic radiation model and its applications, *Adv. Space. Res.*, *17*(2), 7–17, doi:10.1016/0273-1177(95)00507-B.

Chenette, D. L., et al. (1994), The CRRES/SPACERAD heavy ion model of the environment (CHIME) for cosmic ray and solar particle effects on electronic and biological systems in space, *IEEE Trans. Nucl. Sci.*, *41*(6), 2332–2339, doi:10.1109/23.340584.

Cowsik, R., Y. Pal, S. N. Tandon, and R. P. Verma (1967), Steady state of cosmic-ray nuclei—Their spectral shape and path length at low energies, *Phys. Rev.*, *158*(5), 1238–1242, doi:10.1103/PhysRev.158.1238.

Davis, A. J., et al. (2001), Solar minimum spectra of galactic cosmic rays and their implications for models of the near-earth radiation environment, *J. Geophys. Res.*, *106*(A12), 29,979–29,987, doi:10.1029/2000JA000325.

Dodd, P. E., et al. (2007), Impact of heavy ion energy and nuclear interactions on single-event upset and latchup in integrated circuits, *IEEE Trans. Nucl. Sci.*, *54*(6), 2303–2311, doi:10.1109/TNS.2007.909844.

Durante, M., and F. A. Cucinotta (2008), Heavy ion carcinogenesis and human space exploration, *Nat. Rev. Cancer.*, *8*(6), 465–472, doi:10.1038/nrc2391.

Durante, M., and F. A. Cucinotta (2011), Physical basis of radiation protection in space travel, *Rev. Mod. Phy.*, *83*, 1245–1281, doi:10.1103/RevModPhys.83.1245.

Fichtner, H. (2005), Cosmic rays in the heliosphere: Progress in the modelling during the past 10 years, *Adv. Space. Res.*, *35*(4), 512–517, doi:10.1016/j.asr.2005.01.012.

Garcia-Munoz, M., G. M. Mason, J. A. Simpson, and J. P. Wefel (1977), Charge and energy spectra of heavy cosmic rays at intermediate energies, in *Proc. 15th Int. Cosmic Ray Conf. (Plovdiv)*, vol. 1, pp. 230–235, Plovdiv, Bulgaria.

George, J. S., et al. (2009), Elemental composition and energy spectra of galactic cosmic rays during solar cycle 23, *Astrophys. J.*, *698*(2), 1666–1681, doi:10.1088/0004-637X/698/2/1666.

Goring, D. G., and V. A. Nikora (2002), Despiking acoustic doppler velocimeter data, *J. Hydraul. Eng.*, *128*(1), 117–126, doi:10.1061/(ASCE)0733-9429(2002)128:1(117).

Jokipii, J. R. (1990), The anomalous component of cosmic rays, in *Physics of the Outer Heliosphere*, edited by S. Grzedzielski and D. E. Page, pp. 169–178, Pergamon Press, Oxford.

Jokipii, J. R., and D. A. Kopriva (1979), Effects of particle drift on the transport of cosmic rays. III - Numerical models of galactic cosmic-ray modulation, *Astrophys. J.*, *234*, 384–392, doi:10.1086/157506.

Klecker, B. (1995), The anomalous component of cosmic rays: Review and new results from SAMPEX, *Nucl. Phys. B Proc. Suppl.*, *39*(1), 94–102, doi:10.1016/0920-5632(95)00011-W.

Kota, J., and J. R. Jokipii (1983), Effects of drift on the transport of cosmic rays. VI - A three-dimensional model including diffusion, *Astrophys. J.*, *265*, 573–581, doi:10.1086/160701.

Mason, G. M., J. E. Mazur, J. R. Dwyer, D. V. Reames, and T. T. von Rosenvinge (1997), New spectral and abundance features of interplanetary heavy ions in corotating interaction regions, *Astrophys. J. Let.*, *486*(2), L149–L152, doi:10.1086/310845.

Mason, G. M., R. A. Leske, M. I. Desai, C. M. S. Cohen, J. R. Dwyer, J. E. Mazur, R. A. Mewaldt, R. E. Gold, and S. M. Krimigis (2008), Abundances and energy spectra of corotating interaction region heavy ions observed during solar cycle 23, *Astrophys. J.*, *678*(2), 1458–1470, doi:10.1086/533524.

McDonald, F. B. (1998), Cosmic-ray modulation in the heliosphere—A phenomenological study, *Space Sci. Rev.*, *83*, 33–50, doi:10.1023/A:1005052908493.

Mewaldt, R., C. Cohen, G. M. Mason, D. Haggerty, and M. Desai (2007), Long-term fluences of solar energetic particles from H to Fe, *Space Science Reviews*, *130*, 323–328, doi:10.1007/s11214-007-9200-8.

Mewaldt, R. A., et al. (2010), Record-setting cosmic-ray intensities in 2009 and 2010, *Astrophys. J. Let.*, *723*(1), L1—L6, doi:10.1088/2041-8205/723/1/L1.

Nymmik, R. A., and A. A. Suslov (1995), Characteristics of galactic cosmic ray flux lag times in the course of solar modulation, *Adv. Space. Res.*, *16*(9), 217–220, doi:10.1016/0273-1177(95)00338-F.

Nymmik, R. A., M. I. Panasyuk, T. I. Pervaja, and A. A. Suslov (1992), A model of galactic cosmic ray fluxes, *Int. J. Radiat. Appl. Instrum. Part D*, *20*(3), 427–429, doi:10.1016/1359-0189(92)90028-T.

O'Neill, P. M. (2006), Badhwar O'Neill galactic cosmic ray model update based on advanced composition explorer (ACE) energy spectra from 1997 to present, *Adv. Space. Res.*, *37*, 1727–1733, doi:10.1016/j.asr.2005.02.001.

O'Neill, P. M. (2010), Badhwar O'Neill 2010 galactic cosmic ray flux model—Revised, *IEEE Trans. Nucl. Sci.*, *57*(6), 3148–3153, doi:10.1109/TNS.2010.2083688.

Paouris, E., H. Mavromichalaki, A. Belov, R. Gushchina, and V. Yanke (2012), Galactic cosmic ray modulation and the last solar minimum, *Solar. Phys.*, *280*(1), 255–271, doi:10.1007/s11207-012-0051-4.

Pei, C., J. W. Bieber, R. A. Burger, and J. Clem (2010), A general time-dependent stochastic method for solving Parker's transport equation in spherical coordinates, *J. Geophys. Res.*, *115*, A12107, doi:10.1029/2010JA015721.

Qin, G., M. Zhang, and J. R. Dwyer (2006), The effect of adiabatic cooling on the fitted parallel mean free path of solar energetic particles, *J. Geophys. Res.*, *111*, A08101, doi:10.1029/2005JA011512.

Qin, G., L.-L. Zhao, and H.-C. Chen (2012), Despiking of spacecraft energetic proton flux to study galactic cosmic-ray modulation, *Astrophys. J.*, *752*(2), 138, doi:10.1088/0004-637X/752/2/138.

Sierawski, B. D., M. H. Mendenhall, R. A. Reed, R. A. Adams, J. H. Watts, and J. W. Barghouty (2010), CRÈME-MC: A physics-based single event effects tool, in *Nuclear Science Symposium Conference Record (NSS/MIC), 2010*, pp. 1258–1261, IEEE, United States. doi:10.1109/NSSMIC.2010.5873968.

Stone, E. C., A. M. Frandsen, R. A. Mewaldt, E. R. Christian, D. Margolies, J. F. Ormes, and F. Snow (1998a), The advanced composition explorer, *Space. Sci. Rev.*, *86*, 1–22, doi:10.1023/A:1005082526237.

Stone, E. C., et al. (1998b), The cosmic-ray isotope spectrometer for the advanced composition explorer, *Space. Sci. Rev.*, *86*, 285–356, doi:10.1023/A:1005075813033.

Stone, E. C., et al. (1998c), The solar isotope spectrometer for the advanced composition explorer, *Space. Sci. Rev.*, *86*, 357–408, doi:10.1023/A:1005027929871.

Tylka, A. J., J. H. Adams, P. R. Boberg, B. Brownstein, W. F. Dietrich, E. O. Flueckiger, E. L. Petersen, M. A. Shea, D. F. Smart, and E. C. Smith (1997), CRÈME96: a revision of the cosmic ray effects on micro-electronics code, *IEEE Trans. Nucl. Sci.*, *44*(6), 2150–2160, doi:10.1109/23.659030.

Usoskin, I. G., G. A. Bazilevskaya, and G. A. Kovaltsov (2011), Solar modulation parameter for cosmic rays since 1936 reconstructed from ground-based neutron monitors and ionization chambers, *J. Geophys. Res.*, *116*, A02104, doi:10.1029/2010JA016105.

Weller, R. A., M. H. Mendenhall, R. A. Reed, R. D. Schrimpf, K. M. Warren, B. D. Sierawski, and L. W. Massengill (2010), Monte Carlo simulation of single event effects, *IEEE Trans. Nucl. Sci.*, *57*, 1726–1746, doi:10.1109/TNS.2010.2044807.

Wiedenbeck, M. E., et al. (2005), The level of solar modulation of galactic cosmic rays from 1997 to 2005 as derived from ACE measurements of elemental energy spectra, in *Proc. 29th Int. Cosmic Ray Conf. (Pune)*, vol. 2, pp. 277–280, Pune, India.

Wilson, J. W., F. A. Cucinotta, H. Taim, L. C. Simonsen, J. L. Shinn, S. A. Thibeault, and M. Y. Kim (1997), Galactic cosmic ray shielding in deep space , in *NASA Tech. Pap.*, vol. 3682, 23 pp., NASA Langley Research Center, Hampton, Va.

Zhang, M. (1999), A Markov stochastic process theory of cosmic-ray modulation, *Astrophys. J.*, *513*(1), 409–420, doi:10.1086/306857.